

# Geophysical Research Letters

## RESEARCH LETTER

10.1029/2018GL077723

### Special Section:

New understanding of the solar eclipse effects on geospace: The 21 August 2017 Solar Eclipse

### Key Points:

- Ionospheric depletions were generated in the path of totality, and extended effects driven by thermosphere/ionosphere interactions were simulated globally
- Mesospheric ozone and atomic oxygen responses followed the path of totality, with nearly a factor of 2 increase in ozone
- Perturbations propagating from the lower atmosphere have a significant effect on the ionosphere in the aftermath of the eclipse

### Correspondence to:

J. M. McInerney,  
joemci@ucar.edu

### Citation:

McInerney, J. M., Marsh, D. R., Liu, H.-L., Solomon, S. C., Conley, A. J., & Drob, D. P. (2018). Simulation of the 21 August 2017 solar eclipse using the Whole Atmosphere Community Climate Model-eXtended. *Geophysical Research Letters*, 45, 3793–3800. <https://doi.org/10.1029/2018GL077723>

Received 28 FEB 2018

Accepted 11 APR 2018

Accepted article online 23 APR 2018

Published online 5 MAY 2018

## Simulation of the 21 August 2017 Solar Eclipse Using the Whole Atmosphere Community Climate Model-eXtended

Joseph M. McInerney<sup>1</sup> , Daniel R. Marsh<sup>1,2</sup> , Han-Li Liu<sup>1</sup> , Stanley C. Solomon<sup>1</sup> , Andrew J. Conley<sup>2</sup> , and Douglas P. Drob<sup>3</sup> 

<sup>1</sup>High Altitude Observatory, National Center for Atmospheric Research, Boulder, CO, USA, <sup>2</sup>Atmospheric Chemistry and Modeling Lab, National Center for Atmospheric Research, Boulder, CO, USA, <sup>3</sup>Space Science Division, Naval Research Laboratory, Washington, DC, USA

**Abstract** We performed simulations of the atmosphere-ionosphere response to the solar eclipse of 21 August 2017 using the Whole Atmosphere Community Climate Model-eXtended (WACCM-X v. 2.0) with a fully interactive ionosphere and thermosphere. Eclipse simulations show temperature changes in the path of totality up to  $-3$  K near the surface,  $-1$  K at the stratopause,  $\pm 4$  K in the mesosphere, and  $-40$  K in the thermosphere. In the  $F$  region ionosphere, electron density is depleted by about 55%. Both the temperature and electron density exhibit global effects in the hours following the eclipse. There are also significant effects on stratosphere-mesosphere chemistry, including an increase in ozone by nearly a factor of 2 at 65 km. Dynamical impacts of the eclipse in the lower atmosphere appear to propagate to the upper atmosphere. This study provides insight into coupled eclipse effects through the entire atmosphere from the surface through the ionosphere.

**Plain Language Summary** We used a computer model called the Whole Atmosphere Community Climate Model-eXtended (WACCM-X v. 2.0) to investigate what happens to the atmosphere from the surface of Earth up to space during the “Great American Eclipse” of 21 August 2017. During the eclipse, for a location in the path of totality, the model produces different changes in temperature from the ground up to hundreds of kilometers, with the largest decrease in temperature around 250 km. Also, at this altitude, the electron density of the ionosphere decreases by about 55% during the eclipse. Later on during the day of the eclipse, we see changes not only near the eclipse path but also all over the world. The chemistry in the atmosphere is also affected by the eclipse, including an increase in ozone in the middle atmosphere. Finally, changes that happen in the lower atmosphere affect what happens in space after the eclipse is over. This study helps us to understand how an eclipse can affect both the atmosphere and ionosphere, and how these changes are coupled together.

### 1. Introduction

The “Great American Eclipse” on 21 August 2017 was the most thoroughly observed such event in history, as it presented an accessible venue for solar coronal measurements and viewing by the general public. It also offered a unique opportunity to study the upper atmosphere and ionosphere response to transient and localized changes in solar radiation. Many observations of these effects were conducted along and near the path of totality, particularly of the ionosphere, and model predictions conducted before the event (e.g., Huba & Drob, 2017) motivated interest in obtaining a mechanistic understanding of eclipse dynamics. Here we present model simulations of the coupled ionosphere-atmosphere response, for their utility in interpretation of the many measurements. In particular, we wish to elucidate how the ionosphere is driven by neutral atmosphere changes not only by the thermosphere in which it is embedded but also by perturbations propagating out of the lower and middle atmosphere.

Interest in eclipse effects in the ionosphere began almost as soon as its discovery; early work was reviewed by Rishbeth (1968). The 7 March 1970 eclipse was noteworthy because it was extensively investigated by several suborbital experiments, ground-based observations, and theoretical calculations, described in a special issue of the *Journal of Atmospheric and Terrestrial Physics* (April 1972). Modeling of neutral thermosphere effects (e.g., Ridley et al., 1984; Roble et al., 1986, and references therein) followed later, and more recent studies have emphasized the complexity of the coupled system (e.g., Le et al., 2008). Investigations focusing on

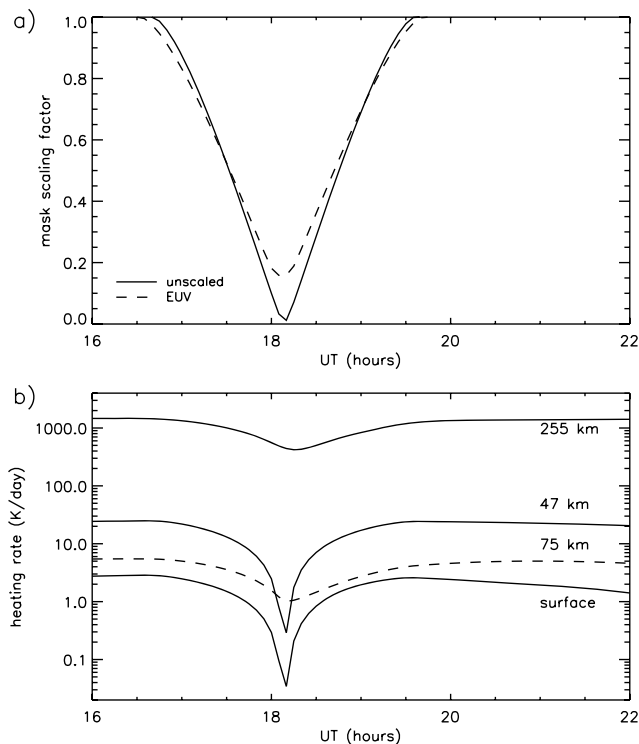


**Figure 1.** (a) The solar eclipse mask factor as a function of UT at latitude  $38.8^\circ$  north and longitude  $95.0^\circ$  west for the unscaled mask near the surface (solid) and the EUV scaled mask at an altitude of 255 km (dashed). (b) Total heating in the model, at the same location, near the surface, and at 47, 75, and 255 km altitude.

the 2017 eclipse have found intriguing evidence of widespread effects suggestive of atmospheric interactions on multiple scales driving ionospheric observables (e.g., Cherniak & Zakharenkova, 2018; Coster et al., 2017; Reinisch et al., 2018; Sun et al., 2018; Zhang et al., 2017). This motivates the modeling studies described in this letter, using a model of the entire atmosphere that includes a fully coupled ionosphere, self-consistent electrostatics, and complete ion-neutral energetics.

## 2. Model Description

There are only a few global general circulation models that can represent the Earth's atmosphere from the surface up to the exosphere, including the Ground-to-topside model of Atmosphere and Ionosphere for Aeronomy (GAIA; Miyoshi & Fujiwara, 2003) and the Whole Atmosphere Model (WAM; Akmaev et al., 2008; Fuller-Rowell et al., 2008). Whole Atmosphere Community Climate Model-eXtended (WACCM-X) is a self-consistent 3-D whole atmosphere global general circulation model extending from the surface to  $\sim 600$  km. The first release of WACCM-X 1.0 in 2012 (Liu et al., 2010) as part of the Community Earth System Model (CESM; Hurrell et al., 2013) extended the neutral atmosphere in altitude, but only included a partial representation of the ionosphere. Recently, electrostatics, ion transport, major and minor neutral species composition, electron and ion density and composition, and electron and ion temperature have been incorporated into WACCM-X to produce a new version (v. 2.0) capable of realistic simulation of ionospheric dynamics and energetics (H.-L. Liu et al., 2018). The basis of this was the National Center for Atmospheric Research (NCAR) Thermosphere-Ionosphere-Electrodynamics General Circulation Model (TIE-GCM; Qian et al., 2014; Richmond et al., 1992). The new version of WACCM-X is also based on the physics and chemistry of the Community Atmosphere Model version 4 (CAM4) and the

Whole Atmosphere Community Climate Model (WACCM) version 4 (WACCM4; Marsh et al., 2013; Neale et al., 2013). WACCM-X has a standard resolution that is  $1.9^\circ \times 2.5^\circ$  latitude  $\times$  longitude and 0.25 scale height in the vertical above 1 hPa, using a log-pressure coordinate system. The upcoming release of the CESM will include WACCM-X 2.0 (see H.-L. Liu, Bardeen, et al., 2018, and J. Liu, Liu, et al., 2018, for further details). For this study, we use this latest version of the model in free-running mode to examine the effects of the 21 August 2017 total solar eclipse from the surface through the thermosphere and ionosphere.

## 3. Eclipse Simulations

To simulate the effects of the eclipse using WACCM-X, we first perform a model spin-up, with initial conditions from 1 August 2005, using low solar activity conditions ( $F_{10.7} = 84$  and  $Kp = 1$ ), and run for 20 days up to the beginning of the eclipse day. A baseline simulation is then performed, starting from the end of the spin-up run. The impact of the eclipse shadow on the solar inputs to the model is incorporated using eclipse masks developed by D. P. Drob. Two masks are used in this study: an "unscaled" mask with an effective solar radius of 1.0, representative of infrared, visible, and near-ultraviolet fluxes, and a "scaled" mask for the extreme-ultraviolet (EUV) spectral region, using an effective solar radius of 1.125 (Huba & Drob, 2017). An example of the reduction in solar flux from these two masks at a point in the path of totality is shown in Figure 1a. The maximum reduction is greater in the unscaled mask than the scaled mask because the solar corona is never fully occulted in the latter. The unscaled mask is applied to three atmospheric processes in the model: solar flux input to the radiative transfer used in the lower atmosphere, the carbon dioxide near-infrared heating rate, and direct photolysis heating. The scaled EUV mask is applied to all photoionization and photodissociation reaction rates, and to direct EUV heating, including photoelectron heating, of the ambient electron gas. Figure 1b shows the change in heating rates at four levels in the atmosphere at the same location as Figure 1a, with all heating and ionization rates adjusted using the appropriate mask. Also,

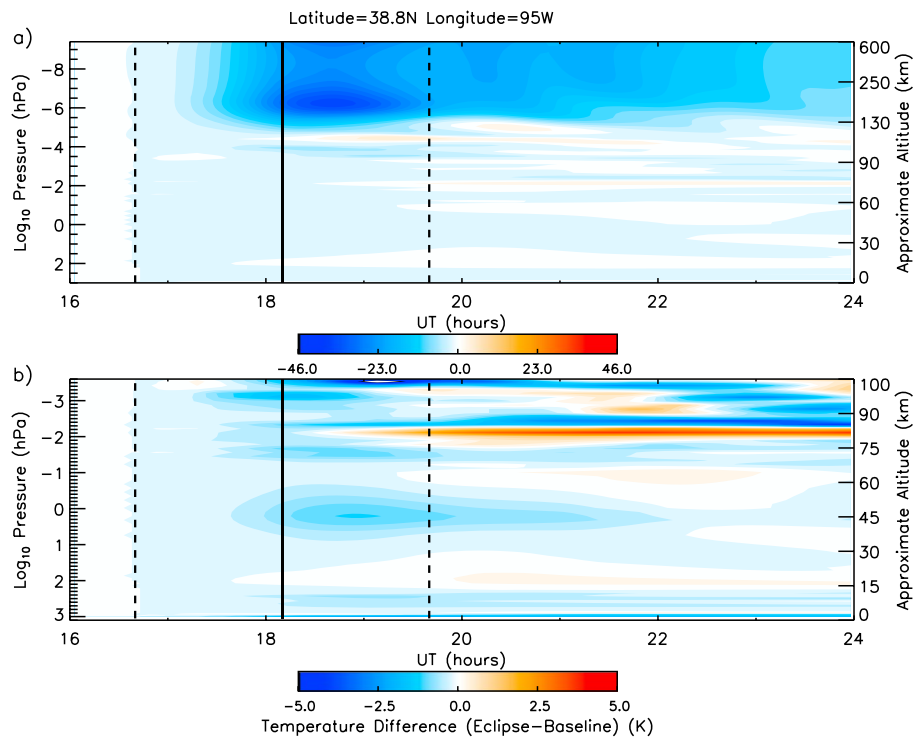


**Figure 2.** Temperature differences between the eclipse and baseline simulations as a function of UT and altitude at a latitude of 38.8° north and a longitude of 95.0° west. (a) Entire model vertical range up to 600 km. (b) Surface to 100 km only. The dashed vertical lines denote the start and end of the eclipse, and the solid vertical lines indicate totality.

each of these heating and ionization processes was evaluated with separate runs, in order to investigate the individual contributions to the total effect on temperature and electron density. We compare the differences between these simulations and the aforementioned baseline simulation, in order to examine global eclipse impacts throughout the atmosphere.

#### 4. Results

Through comparison of simulations using the eclipse mask to the baseline simulation, eclipse effects can be studied in detail, and the impact of individual heat sources can be evaluated. Figure 2 displays temperature differences between eclipse and baseline simulations at 39°N latitude and 95°W longitude as a function of universal time (UT) between 16 UT and 24 UT. In Figure 2a, the y axis is the full vertical range of the model from the ground to 600 km, and in Figure 2b, a subset of this vertical range up to 100 km. The first sign of the eclipse shadow is clear just before 17 UT, when slight cooling begins at all levels. The largest cooling (~40 K) is seen in the thermosphere ( $\sim 3 \times 10^{-7}$  hPa) around 18:45 UT, about 20 min after totality. In the vertical altitude range of 0–100 km, the maximum cooling due to the eclipse near the surface and near the stratosphere is –3 and –1 K, respectively. In the mesosphere, the temperature oscillates with magnitudes up to  $\pm 4$  K.

With the fully interactive chemistry in WACCM-X, we can examine effects on chemical species during the eclipse. Figure 3 shows the percent changes of atomic oxygen and ozone at 65 km and 18 UT over North America during the eclipse relative to the baseline. This is when the path of totality had reached 40.5°N and 98.2°W, over the central United States. There is a clear depletion of atomic oxygen of ~75%, corresponding to ~95% enhancement of ozone.

Turning to the thermosphere-ionosphere, Figure 4 shows global maps of temperature and electron density near 250 km altitude. The left column is at 18:15 UT, when the total solar eclipse was over the central United States, and the right column is at 23:30 UT, over 3 hr after the eclipse ended over the Atlantic Ocean. In Figures 4a and 4b, we show thermospheric temperature. In Figure 4a, there is a clear cooling at

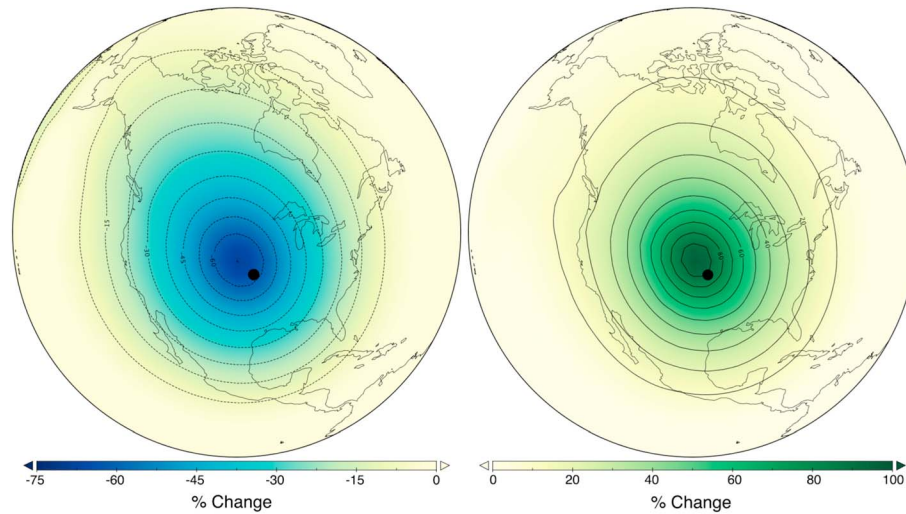


**Figure 3.** The percent differences between eclipse and baseline simulations over North America at an altitude of 65 km of atomic oxygen (left) and ozone (right) at 18:00 UT. The black dots indicate the location of totality.

the location of the total eclipse, less so in the surrounding shadowed regions, extending back along the path of totality. The changes in other parts of the globe are smaller. In Figure 4b, the same projection ~5 hr later, we see eclipse effects of similar magnitude that have become global, including a wave-like signature propagating southward and eastward away from the path of totality. Figures 4c and 4d are electron density at the ionosphere F2 peak (NmF2). During the eclipse at 18:15 UT (Figure 4c), there is a clear NmF2 depletion with a maximum of  $\sim 1.8 \times 10^{-5} \text{ cm}^{-3}$ ,  $\sim 55\%$ , in a pattern similar to temperature, also extending back along the path of totality. Additionally, there are small effects on NmF2 at other locations, with some slight increases to the south and west of the path of totality. Figure 4d, at 23:30 UT, the NmF2 effects have spread globally, with depletions and enhancements about the same order of magnitude as during the

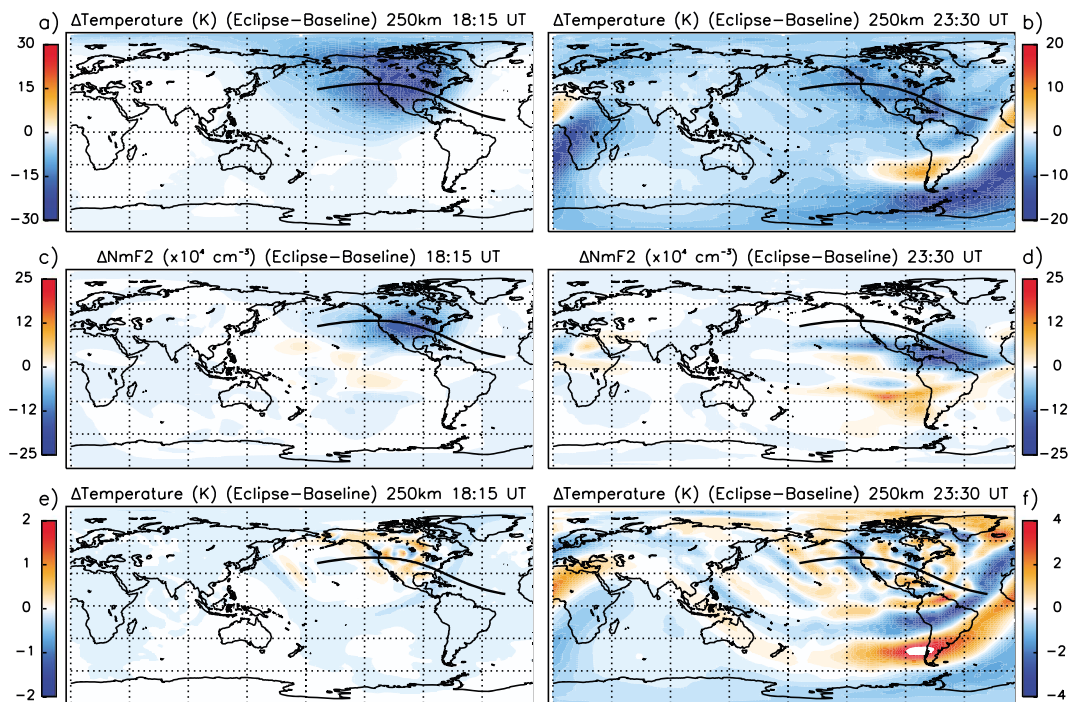


**Figure 4.** (a and b) Global maps of temperature differences at 250 km, eclipse minus baseline, at 18:15 UT and 23:30 UT. (c and d) Electron density differences at the F2 peak. (e and f) Same as (a and b) except with eclipse mask only applied to lower atmosphere heating. The solid lines are the eclipse path of totality.

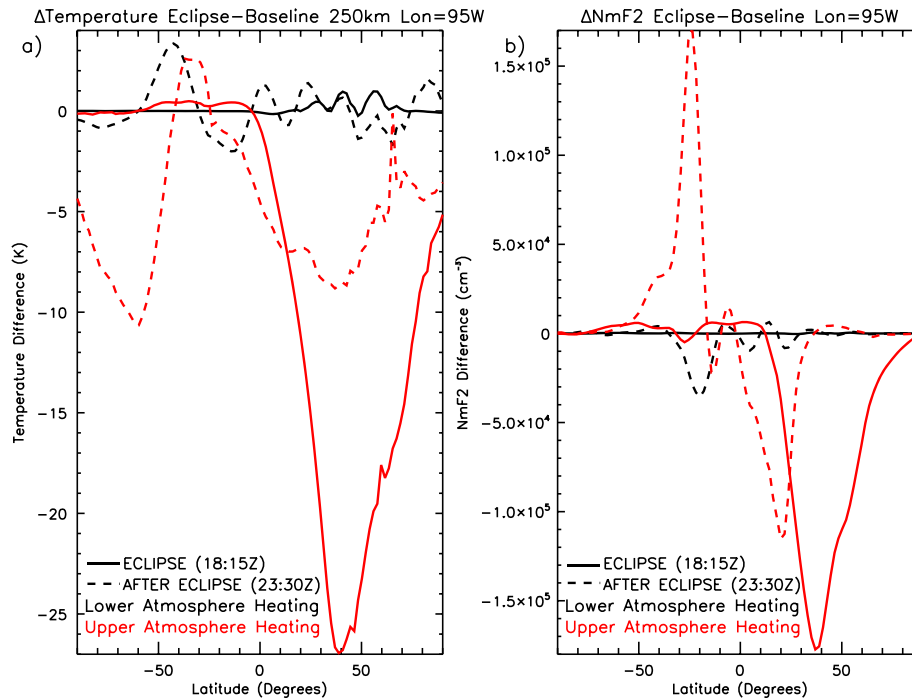


**Figure 5.** (a) Temperature differences and (b) NmF2 differences between eclipse and baseline simulations, as a function of latitude, at longitude 95.0° west and altitude 250 km. Shown are the sum of differences with the eclipse mask applied to lower and middle atmosphere heating (black) and the sum of differences with the eclipse mask applied to middle and upper atmosphere heating (red) for during the eclipse at 18:15 UT (solid) and near the end of the day of the eclipse at 23:30 UT (dashed).

eclipse. In contrast to temperature, which has the eclipse effects propagating somewhat radially away from the path of totality, the NmF2 effects propagate more meridionally than zonally.

We can evaluate eclipse effects in the thermosphere caused by lower atmosphere perturbations by looking at the temperature differences at this same altitude, but for a simulation in which the eclipse mask is applied only to troposphere/stratosphere heating and not to the other heating or ionizing sources. These temperature differences, which are shown in Figures 4e and 4f, are an order of magnitude smaller than those in Figures 4a and 4b. In Figure 4e, during the eclipse at 18:15 UT, there are localized changes in temperature of about 1–2 K near the path of totality, but no clear signature of the path as seen in the top left panel. Since, in this simulation, only lower atmosphere heating is affected by the eclipse passage, this implies that variability propagating from below is causing differences in the thermosphere. In Figure 4f, at 23:30 UT, the effects have spread to nearly all latitudes and longitudes with even larger magnitudes than in Figure 4e and a wave pattern similar to Figure 4b.

To further explore the lower atmosphere eclipse effects on the thermosphere-ionosphere, we show in Figure 5 the temperature differences (left) and NmF2 differences (right), for cases where only lower atmosphere heating was masked and where only upper atmosphere (EUV-driven) heating was masked. The differences are displayed as a function of latitude, at 250 km altitude, for a time during the eclipse at 18:15 UT (solid) and after the end of the eclipse at 23:30 UT (dashed). Direct upper atmosphere heating results in the largest effects (red) during and after the eclipse. However, lower atmosphere heating eclipse effects (black) are nonnegligible in thermosphere temperature and, even more so, in NmF2, particularly after the eclipse in the southern hemisphere. The detection of a lower atmosphere influence on the thermosphere-ionosphere is an important result made possible by this whole atmosphere simulation.

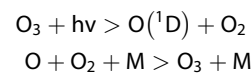
## 5. Discussion and Conclusions

Using the capability of the WACCM-X model to simulate the entire atmosphere, we examine the effects of the 21 August 2017 eclipse from the Earth’s surface up to 600 km. For temperature, at a location over the central United States, we see cooling near the surface, near the stratopause, and in the middle thermosphere, all on

the order of 1–40 K. The cooling near the surface during the eclipse is as much as ~3 K, in the range of that seen from National Weather Service observations during the eclipse (e.g., [https://www.weather.gov/lx/08\\_21\\_2017](https://www.weather.gov/lx/08_21_2017)). The 40 K cooling at ~250 km is similar to the 40 K cooling at 240 km from a study of the 1999 eclipse by Mueller-Wodarg et al. (1998) using the Coupled Thermosphere-Ionosphere-Plasmasphere (CTIP) model. Ridley et al. (1984) reported a maximum 70 K cooling at 300 km during the 1983 eclipse and Roble et al. (1986) found a 57 K cooling at ~250 km during the 1984 eclipse, both using the Thermosphere General Circulation Model. These comparisons illustrate that WACCM-X compares well with previous results in the upper atmosphere and also provides a comprehensive understanding of eclipse effects throughout the atmosphere.

When the eclipse mask is applied only to lower atmosphere heating, we still see effects on the temperature at 250 km during and after the eclipse, as shown in Figure 4. This is further illustrated in Figure 5, where temperature and NmF2 both show significant posteclipse effects. Although much smaller than the more direct effect of EUV change in the thermosphere-ionosphere, these are indications that eclipse effects in the lower atmosphere contribute to variability in the upper atmosphere for many hours after the eclipse.

With the inclusion of interactive chemistry in WACCM-X, we examined the effects on atomic oxygen and ozone in the mesosphere, noting in Figure 3 a 75% depletion and 95% enhancement, respectively. Further examination of the chemistry involved gives insight into these changes. In this part of the atmosphere the two main reactions affecting the abundances of ozone and atomic oxygen are



The first of these reactions results in the destruction of ozone by photolysis. The second is the production of ozone by the recombination of atomic and molecular oxygen. During the eclipse, with the reduction of incoming solar radiation, the first photolysis reaction is decreased significantly, no longer destroying ozone at the rate typically seen during daytime, while the second reaction continues producing ozone, at the expense of atomic oxygen. The result is a decrease of atomic oxygen and an increase of ozone during the eclipse shown in Figure 3. This will change heating and cooling rates in the vicinity of the eclipse path and could contribute to dynamical perturbations propagating into the thermosphere, but additional experimentation and analysis will be needed to disentangle effects caused by middle atmosphere chemistry from those driven by lower atmosphere temperature changes.

Global maps during the eclipse show both the temperature decrease at 250 km and depletion of NmF2 extend back along the path of totality, as seen in Coster et al. (2017). Depletion of WACCM-X NmF2 over a broad area under the eclipse shadow has a maximum of ~55% at 250 km near the eclipse center. This is comparable to, but clearly larger than, the prediction from Huba and Drob (2017) of a 30% electron density decrease at 306 km. Since eclipse effects on electron column density in the WACCM-X model are dominated by depletion in the NmF2 region, this 55% decrease can be compared to observations of total electron content (TEC). During the 2017 eclipse, Coster et al. (2017) found a TEC reduction of 50–60% and Sun et al. (2018) observed a reduction of 37–43%. During the 2005 eclipse, a 30% reduction in TEC was reported by Jakowski et al. (2008) and 20–30% by Krankowski et al. (2008).

A modest but widespread enhancement in TEC observed over much of North America in the wake of the eclipse has been reported (e.g., Chorniak & Zakharenkova, 2018). Our model simulations do not produce these enhancements. Since the solar and geomagnetic forcing of the model was held constant, any externally driven day-to-day ionospheric variability would be absent, and it is not known if the observed enhancements were due to solar/geomagnetic variability or eclipse effects. However, in the hours following the eclipse, and even into the next day, a nearly global response is seen in model temperature and NmF2. For temperature at 250 km, a wave-like structure propagates away from the eclipse region. This is similar to what Mueller-Wodarg et al. (1998) predicted for the 1999 eclipse, and Zhang et al. (2017) describe large-scale ionospheric perturbations in observations of TEC after the eclipse. The most salient feature seen in the model NmF2 are differences in the hours following the eclipse in the equatorial region that have no clear connection back to the eclipse path of totality. These NmF2 differences are slightly smaller than the depletion during the eclipse. They occur along the geomagnetic equator in the equatorial ionization anomaly region of both hemispheres, even extending into the southern hemisphere midlatitudes. These NmF2 changes in the equatorial region might result from changes in neutral winds near the path of totality that propagate to lower latitudes. This

could induce a disturbance in equatorial electrodynamics, modifying the “fountain” effect responsible for the equatorial ionization anomaly. A mechanism of this type would explain why the NmF2 differences follow the geomagnetic, rather than the geographic, equator.

As seen in Figure 2, a time lag occurs in WACCM-X temperature between the actual passage of the eclipse at 18:15 UT and the largest temperature changes around 19:00 UT, ~45 min after the time of totality. The previously described study by Mueller-Wodarg et al. (1998) concluded that the temperature minimum at 240 km would lag the passage of the total eclipse by 30 min. In the case of TEC, we found that the lag for WACCM-X electron column density at one location is ~15 min. During the 2017 eclipse, the lag between total obscuration and maximum TEC reduction is reported by Coster et al. (2017) to be 10 min, Sun et al. (2018) to be several minutes to half an hour, and Cherniak and Zakharenkova (2018) to be ~8–20 min. For the 2005 eclipse, Jakowski et al. (2008) and Krankowski et al. (2008) found this lag in TEC of 20–30 min. These relatively short lags in TEC are commensurate with ionospheric chemical recombination and diffusion lifetimes, whereas the slower heat conductance at thermospheric altitudes results in a more sluggish temperature response

These results from whole atmosphere WACCM-X simulations demonstrate that the thermosphere-ionosphere system responds not only along the path of totality of the eclipse but also globally, to the local perturbation induced by the “Great American Eclipse” and indicates the need for more thorough investigations into the many atmospheric impacts waiting to be uncovered during this and future total eclipses of the Sun.

#### Acknowledgments

WACCM-X source code and results are publicly available at the NCAR Community Earth System Model website. Model output data used in this letter are archived on the NCAR High Performance Storage System. Simulations were performed using computational resources at the NCAR-Wyoming Supercomputing Center (doi:10.5065/D6RX99HX). Work at NCAR was supported by National Science Foundation grant 1135432 and by NASA grants 80NSSC17K0007, NNX14AH54G, NNX15AJ24G, and NNX16AB82G. Work by D. Drob at the U.S. Naval Research Laboratory was sponsored by NASA grant NNX17AE63L. NCAR is sponsored by the National Science Foundation.

#### References

- Akmaev, R. A., Fuller-Rowell, T. J., Wu, F., Forbes, J. M., Zhang, X., Anghel, A. F., et al. (2008). Tidal variability in the lower thermosphere: Comparison of Whole Atmosphere Model (WAM) simulations with observations from TIMED. *Geophysical Research Letters*, *35*, L03810. <https://doi.org/10.1029/2007GL032584>
- Cherniak, I., & Zakharenkova, I. (2018). Ionospheric total electron content response to the great American solar eclipse of 21 August 2017. *Geophysical Research Letters*, *45*, 1199–1208. <https://doi.org/10.1002/2017GL075989>
- Coster, A. J., Goncharenko, L., Zhang, S.-R., Erickson, P. J., Rideout, W., & Vierinen, J. (2017). GNSS observations of ionospheric variations during the 21 August 2017 solar eclipse. *Geophysical Research Letters*, *44*, 12,041–12,048. <https://doi.org/10.1002/2017GL075774>
- Fuller-Rowell, T. J., Akmaev, R. A., Wu, F., Anghel, A., Maruyama, N., Anderson, D. N., et al. (2008). Impact of terrestrial weather on the upper atmosphere. *Geophysical Research Letters*, *35*, L09808. <https://doi.org/10.1029/2007GL032911>
- Huba, J. D., & Drob, D. (2017). SAMI3 prediction of the impact of the 21 August 2017 total solar eclipse on the ionosphere/plasmasphere system. *Geophysical Research Letters*, *44*, 5928–5935. <https://doi.org/10.1002/2017GL073549>
- Hurrell, J. W., Holland, M. M., Gent, P. R., Ghan, S., Kay, J. E., Kushner, P. J., et al. (2013). The community earth system model: A framework for collaborative research. *Bulletin of the American Meteorological Society*, *94*(9), 1339–1360. <https://doi.org/10.1175/BAMS-D-12-00121.1>
- Jakowski, N., Stankov, S. M., Wilken, V., Borries, C., Altadill, D., Chum, J., et al. (2008). Ionospheric behavior over Europe during the solar eclipse of 3 October 2005. *Journal of Atmospheric and Solar-Terrestrial Physics*, *70*(6), 836–853. <https://doi.org/10.1016/j.jastp.2007.02.016>
- Krankowski, A., Shagimuratov, I. I., Baran, L. W., & Yakimova, G. A. (2008). The effect of total solar eclipse of October 3, 2005, on the total electron content over Europe. *Advances in Space Research*, *41*(4), 628–638. <https://doi.org/10.1016/j.asr.2007.11.002>
- Le, H., Liu, L., Yue, X., & Wan, W. (2008). The ionospheric responses to the 11 August 1999 solar eclipse: Observations and modeling. *Annales Geophysicae*, *26*(1), 107–116. <https://doi.org/10.5194/angeo-26-107-2008>
- Liu, H.-L., Bardeen, C. G., Foster, B. T., Lauritzen, P., Liu, J., Lu, G., et al. (2018). Development and validation of the Whole Atmosphere Community Climate Model with thermosphere and ionosphere extension (WACCM-X). *Journal of Advances in Modeling Earth Systems*, *10*(2), 381–402. <https://doi.org/10.1002/2017MS001232>
- Liu, H.-L., Foster, B. T., Hagan, M. E., McInerney, J. M., Maute, A., Qian, L., et al. (2010). Thermosphere extension of the Whole Atmosphere Community Climate Model. *Journal of Geophysical Research*, *115*, A12302. <https://doi.org/10.1029/2010JA015586>
- Liu, J., Liu, H., Wang, W., Burns, A. G., Wu, Q., Gan, Q., et al. (2018). First Results from the Ionospheric Extension of WACCM-X during the Deep Solar Minimum Year of 2008. *Journal of Geophysical Research: Space Physics*, *123*(2), 1534–1553. <https://doi.org/10.1002/2017JA025010>
- Marsh, D. R., Mills, M. J., Kinnison, D. E., Lamarque, J.-F., Calvo, N., & Polvani, L. M. (2013). Climate change from 1850 to 2005 simulated in CESM1(WACCM). *Journal of Climate*, *26*(19), 7372–7391. <https://doi.org/10.1175/JCLI-D-12-00558.1>
- Miyoshi, Y., & Fujiwara, H. (2003). Day-to-day variations of migrating diurnal tide simulated by a GCM from the ground surface to the exobase. *Geophysical Research Letters*, *30*(15), 1789. <https://doi.org/10.1029/2003GL017695>
- Mueller-Wodarg, I. C. F., Aylward, A. D., & Lockwood, M. (1998). Effects of a mid-latitude solar eclipse on the thermosphere and ionosphere—A modelling study. *Geophysical Research Letters*, *25*, 3787–3790. <https://doi.org/10.1029/1998GL900045>
- Neale, R., Richter, J., Park, S., Lauritzen, P., Vavrus, S., Rasch, P., & Zhang, M. (2013). The mean climate of the Community Atmosphere Model (CAM4) in forced SST and fully coupled experiments. *Journal of Climate*, *26*(14), 5150–5168. <https://doi.org/10.1175/JCLI-D-12-00236.1>
- Qian, L. Y., Burns, A. G., Emery, B. A., Foster, B., Lu, G., Maute, A., et al. (2014). The NCAR TIE-GCM: A community model of the coupled thermosphere/ionosphere system. In J. Huba, R. Schunk, & G. Khazanov (Eds.), *Modeling the ionosphere and thermosphere system*, *Geophysical Monograph Series* (Chap. 7, p. 73). Chichester, UK: John Wiley. <https://doi.org/10.1002/9781118704417.ch7>
- Reinisch, B. W., Dandenault, P. B., Galkin, I. A., Hamel, R., & Richards, P. G. (2018). Investigation of the electron density variation during the August 21, 2017 solar eclipse. *Geophysical Research Letters*, *45*, 1253–1261. <https://doi.org/10.1002/2017GL076572>
- Richmond, A. D., Ridley, E. C., & Roble, R. G. (1992). A thermosphere/ionosphere general circulation model with coupled electrodynamics. *Geophysical Research Letters*, *19*, 601–604. <https://doi.org/10.1029/92GL00401>
- Ridley, E. C., Dickinson, R. E., & Roble, R. G. (1984). Thermospheric response to the June 11, 1983, solar eclipse. *Journal of Geophysical Research*, *89*, 7583–7588. <https://doi.org/10.1029/JA089iA09p07583>

- Rishbeth, H. (1968). Solar eclipses and ionospheric theory. *Space Science Reviews*, 8(4), 543–554. <https://doi.org/10.1007/BF00175006>
- Roble, R. G., Emery, B. A., & Ridley, E. C. (1986). Ionospheric and thermospheric response over millstone-hill to the May 30, 1984, annular solar eclipse. *Journal of Geophysical Research*, 91, 1661–1670. <https://doi.org/10.1029/JA091iA02p01661>
- Sun, Y.-Y., Liu, J.-Y., Lin, C.-H., Lin, C.-Y., Shen, M.-H., Chen, C.-H., et al. (2018). Ionospheric bow wave induced by the moon shadow ship over the continent of United States on 21 August 2017. *Geophysical Research Letters*, 45, 538–544. <https://doi.org/10.1002/2017GL075926>
- Zhang, S.-R., Erickson, P. J., Goncharenko, L. P., Coster, A. J., Rideout, W., & Vierinen, J. (2017). Ionospheric bow waves and perturbations induced by the 21 August 2017 solar eclipse. *Geophysical Research Letters*, 44, 12,067–12,073. <https://doi.org/10.1002/2017GL076054>